SIRIMA

SINKHOLE HAZARD AND RISK MANAGEMENT IN POST MINING AREAS

RFCS PROJECT NO 101157400

Co-funded by the European Union

Deliverable D.4.1

Presentation of the method and 1st results of the interferometric processing phase on the identified site of Thil (France)

WP.4. Sinkhole hazards and risks related to shallow mine workings

Responsible Partner**:** Bureau de recherches géologiques et minières - BRGM, France

Contributing Partners:

1. Główny Instytut Górnictwa Państwowy Instytut Badawczy, Poland
2. DMT - Technische Hochschule Georg Agricola, Germany

Authors: Aya Cheaib, Daniel Raucoules, Marcello De Michele.

This Deliverable has been made as a result of the SIRIMA project – Sinkhole hazard and risk management in post mining areas.

December, 2025

Table of contents

1. Introduction 5

2. Principles of Synthetic Aperture Radar Interferometry (InSAR) 7

3. Study sites 8

4. Working strategy and datasets 10

5. InSAR methods applied for Thil test site 10

5.1. SBAS 12

5.2. Persistent Scatterer Interferometry with Interferometric Point Target Analysis (IPTA) 12

6. Preliminary results on Thil test site 14

7. The introduction of a new study site in France: Saint-Etienne mining site 22

8. Conclusions and perspectives 23

References 25

List of figures

Figure 1: Graphical presentation of the Partners in the SIRIMA project. 6
Figure 2: Mining sites studied with InSAR in the SIRIMA project 9
Figure 3: (A) Location of the Thil mine. (B) Zoom on the mining area showing the monitored section of the site. (C) Detailed view of the underground layout, highlighting accessible pillars and collapsed mining areas. 11
Figure 4: Temporal and perpendicular baselines of the generated Sentinel-1 interferograms for both SBAS and IPTA processing over the study area, showing the interferogram network of (a) 6-, 12-, 18-, and 24-day intervals, and (b) 1-year interval 13
Figure 5: LOS mean velocity map for the 2015–2025 period obtained with SBAS processing. Negative values indicate motion away from the satellite. The zoomed areas correspond to the regions shown in Figures 9, 12, and 15. 14
Figure 6: LOS mean velocity map for the 2015–2025 period obtained with SBAS processing, overlaid with the available underground mine layout with the risk zones identified by the DPSM. Negative values indicate motion away from the satellite 15
Figure 7 : LOS mean velocity map for the 2015–2025 period obtained with IPTA processing. Negative values indicate motion away from the satellite. The zoomed areas correspond to the regions shown in Figures 10, 13, and 16. 15
Figure 8: LOS mean velocity map for the 2015–2025 period obtained with IPTA processing, overlaid with the available underground mine layout with the risk zones identified by the DPSM. Negative values indicate motion away from the satellite 16
Figure 9: Zoom showing the LOS mean velocity map for the 2015–2025 period obtained from SBAS processing, overlaid with the monitored section of the Thil mine and the risk zones. The location of this zoomed area is indicated by polygon 1 in Figure 5. 17
Figure 10: Zoom showing the LOS mean velocity map for the 2015–2025 period obtained with IPTA processing, overlaid with the monitored section of the Thil mine and the risk zones. The location of this zoomed area is indicated by polygon 1 in Figure 7. Points a, b and c indicate the locations of the time series presented in Figure 11. 18
Figure 11: Time series plots showing the cumulative LOS displacement for points a, b and c indicated in Figure 10. 18
Figure 12: Zoom showing the LOS mean velocity map for the 2015–2025 period obtained from SBAS processing, overlaid with the available underground mine layout and the risk zones. The location of this zoomed area is indicated by polygon 2 in Figure 5. 19
Figure 13: Zoom showing the LOS mean velocity map for the 2015–2025 period obtained with IPTA processing, overlaid with the available underground mine layout and the risk zones. The location of this zoomed area is indicated by polygon 2 in Figure 7. Points a, b and c indicate the locations of the time series presented in Figure 14. 19

Figure 14: Time series plots showing the cumulative LOS displacement for points a, b and c indicated in Figure 13. 20
Figure 15: Zoom showing the LOS mean velocity map for the 2015–2025 period obtained from SBAS processing, overlaid with the available underground mine layout and the risk zones. The location of this zoomed area is indicated by polygon 3 in Figure 5. 20
Figure 16: Zoom showing the LOS mean velocity map for the 2015–2025 period obtained with IPTA processing, overlaid with the available underground mine layout and the risk zones. The location of this zoomed area is indicated by polygon 3 in Figure 7. Points a, b and c indicate the locations of the time series presented in Figure 17. 21
Figure 17: Time series plots showing the cumulative LOS displacement for points a, b and c indicated in Figure 16. 21
Figure 18: Persistent scatterers from the European Ground Motion Service at the Saint-Étienne site (ascending tracks 161 and 59 of Sentinel-1 data). Negative values indicate motion away from the satellite 23

List of tables

Table 1 Contact list of persons responsible for the implementation of the SIRIMA project at the Consortium Partners 5

1. Introduction

Document Overview

The SIRIMA: *Sinkhole Hazard and Risk Management in Post-Mining Areas* project is carried out with co-financing from the Research Found for Coal and Steel of the European Union as the action RFCS-2023-01-RPJ Coal Research Projects under Grant Agreement No. 101157400.

This document entitled **"presentation of the method and 1st results of the interferometric processing phase on the identified site of Thil (France)"**, represents the deliverable for Task 4.2 and is denoted as D.4.1. The purpose of this report is to present the advanced satellite Synthetic Aperture Radar Interferometry (InSAR) methods applied within the SIRIMA project for monitoring land surface motion and characterising the spatio-temporal variability of ground deformation related to post-mining activities in shallow coal deposits. These methods will be applied across several study sites (Poland, Germany, and France), while the present document focuses on the first results obtained for the Thil test site in France. The document is organized as follows:

- Introduction (Section 1)
- Principles of Synthetic Aperture radar interferometry (InSAR) (Section 2)
- Study sites (Section 3)
- Working strategy and datasets (Section 4)
- InSAR methods applied for Thil test site (Section 5)
- Preliminary results on Thil test site (Section 6)
- The introduction of a new study site in France: Saint-Etienne mining site (Section 7)
- Conclusions and perspectives (Section 8).

Contributing Partners

The SIRIMA Project Consortium consists of seven Partners and one Associated Partner. The Table 1 below, presents the Consortium participants along with the contact details of the persons responsible for the implementation of the SIRIMA project in their home institutions:

Table 1 Contact list of persons responsible for the implementation of the SIRIMA project at the Consortium Partners

Partner	Full Name	Contact Person	Contact Email
GIG-PIB	Główny Instytut Górnictwa - Państwowy Instytut Badawczy	Sławomir Siwek	ssiwek@gig.eu
INERIS	Institut national de l'environnement industriel et des risques	Isabelle Vuidart	Isabelle.VUIDART@ineris.fr
BRGM	Bureau de recherches géologiques et minières	Pascal Dominique	p.dominique@brgm.fr
DMT	DMT-Gesellschaft fur Lehre und Bildung mbH - THGA	Tobias Rudolph	tobias.rudolph@thga.de

IMG-PAN	Instytut Mechaniki Górotworu - Polskiej Akademii Nauk	Krzysztof Tajduś	tajdus@imgpan.pl
SUBTERRA	Systra Subterra Ingenieria SLU	Beatriz Garcia Bernabeu	bgarcia2@systra.com
UL	Université De Lorraine	Rasool Mehdizadeh	rasool.mehdizadeh@univ-lorraine.fr
GEODERIS	GEODERIS	Pascal Bigarre	pascal.bigarre@geoderis.fr

General Information about Project

The SIRIMA project focuses on increasing knowledge and experience related to the threats of post-mining areas in EU Member States. The main objective of the project is to reduce the occurrence of uncontrolled and unexpected movements of the Earth's surface in the areas of abandoned shallow coal mines. These movements, apart from subsidence related to the conducted mining or movements resulting from the impact of mining tremors, can also take the form of uplifts caused by the lifting of the groundwater table in the rock mass and sudden - discontinuous deformations of the ground surface, i.e. sinkholes. The sinkhole hazard is the main type of hazard affecting coal regions in transition. It is due to existence of shallow mining workings and the resulting risk of damage to the buildings, infrastructure or threat to people living in post-mining areas.

Figure 1: Graphical presentation of the Partners in the SIRIMA project.

2. Principles of Synthetic Aperture Radar Interferometry (InSAR)

Interferometric Synthetic Aperture Radar (InSAR) is a satellite-based geodetic technique that measures ground deformation by comparing the phase information contained in two radar acquisitions acquired at different dates. The phase difference, or interferogram, reflects changes in the radar line-of-sight (LOS) distance and therefore provides a synoptic representation of surface displacements (Massonnet and Feigl, 1998; de Michele et al., 2023). Originally developed for generating digital elevation models (e.g., Small, 1998), InSAR has become an essential tool for detecting and quantifying subtle ground motions associated with natural or anthropogenic processes through Differential InSAR (DInSAR) (Massonnet and Feigl, 1998).

To improve accuracy and temporal continuity from classical DInSAR, multi-temporal InSAR (MT-InSAR) approaches were later introduced, reaching millimetric precision by mitigating atmospheric noise and temporal decorrelation. Among these, the Persistent Scatterer (PS) technique identifies phase-stable radar targets, often buildings or natural reflectors such as bare rock, allowing long-term, high-precision deformation monitoring even for disconnected regions (Ferretti et al., 2001; Hooper et al., 2004). Other methods exploit Distributed Scatterer (DS) targets together with Persistent Scatterers (PS) to increase measurement density and robustness; this type of integrated MT-InSAR processing is used in the European Ground Motion Service (EGMS) to generate ground-motion products at the scale of Europe (Crosetto et al, 2021). In parallel, SBAS (Small Baseline Subset) methods generate spatially continuous deformation fields using networks of interferograms with small spatial and temporal baselines, enabling reliable time series over broad regions where PS densities may be limited (Berardino et al., 2002; Lanari et al., 2004, Doin et al., 2011). These complementary MT-InSAR approaches provide a robust and flexible approach for mapping and analysing a wide spectrum of ground-deformation processes.

By combining different MT-InSAR approaches, it becomes possible to robustly map and analyse diverse ground-deformation processes over the long term with millimetric precision and spatially dense observations. Thanks to these advantages, InSAR has become a fundamental tool across numerous Earth science disciplines. It is widely used for monitoring natural hazards, such as slow-moving landslides (Rosi et al., 2018; Aslan et al., 2020; Cheaib et al., 2022), volcanic inflation and deflation (Biggs and Pritchard, 2017; Albino et al., 2020), and co-seismic and post-seismic deformation (Massonnet et al., 1993; Wright et al., 2001). In addition, MT-InSAR contributes to monitoring anthropogenic ground deformation, such as in post-mining settings, where it enables the detection of residual subsidence or uplift and the reactivation of ground movements long after mining activities have ceased (Raucoules et al., 2007; Herrera et al., 2010, Apanowicz et al., 2025).

A key factor in the widespread adoption of MT-InSAR applications has been the availability of open-access Sentinel-1 SAR data since 2014, acquired at 6- or 12-day intervals. Sentinel-1 is the first in the Copernicus Sentinel series, a high-resolution C-Band radar imagery satellite constellation, providing an all-weather, day-and-night supply of images of Earth's surface. It

belongs to the Copernicus program: the Earth observation component of the European Union's Space program managed by the European commission. It is implemented in partnership with the Member States, the European Space Agency (ESA), the European Organization for the Exploitation of Meteorological Satellites (EUMETSAT), the European Centre for Medium-Range Weather Forecasts (ECMWF), EU Agencies and Mercator Océan, the European Environment Agency (EEA), the Joint Research Centre (JRC).

Limitations of the Technique

The performance of InSAR is limited in densely vegetated or rapidly deforming areas due to temporal and geometric decorrelation, which introduces strong noise when surface properties change between acquisitions (Massonnet and Feigl, 1998; Hanssen, 2001). Additional limitations include phase unwrapping errors for large deformations, and atmospheric artefacts caused by spatially and temporally variable path delays, which can be mistaken for ground motion. Furthermore, InSAR measurements are restricted to the satellite line-of-sight (LOS), meaning that observed displacements represent only a projection of the true three-dimensional ground motion. To accurately separate vertical and horizontal components, data acquired with different incidence angles (ascending and descending acquisitions of Sentinel-1 for example) over the same area are typically required.

3. Study sites

Three distinct shallow mining areas located in France, Germany, and Poland are being monitored using advanced InSAR techniques by the respective partner organizations.

For the French site, BRGM, responsible for coordinating this task, conducts the InSAR processing for the Thil test area, which is presented in this report. Although the Thil site is located within an iron-ore deposit in northeastern France (Fig.2), it was selected for monitoring as it represents a shallow mining environment and has already been the subject of continuous surveillance since 2020. In 1956 then 1957, two sinkholes (called West sinkhole and East sinkhole) were formed in the main gallery of Thil mine, creating an isolated chamber at the bottom of the mine between the two sinkholes. The most recent triannual inspection by the Department for Mine Safety and Risk Prevention (BRGM-DPSM) revealed major roof falls in the western cavity, prompting the implementation of enhanced, continuous monitoring using multifunctional systems such as video, acoustic, vibration, and laser distance sensors (Hervé, 2022). The application of InSAR at this mining site aims to assess potential ground deformation associated with the 2018–2020 roof-fall events and to detect any subsequent surface movements that may indicate ongoing instability.

Two additional shallow hard coal mining sites, Siersza and Kazimierz-Juliusz, in Poland are being monitored using InSAR methods by colleagues from GIG-PIB. The Siersza mine in Trzebinia, liquidated in 1999 through shaft filling and cessation of drainage, has seen groundwater rise to the shallowest mining excavations or above, creating significant sinkhole hazard.

Historically, a few sinkholes occurred each year, but the rate accelerated as groundwater reached the top of the Carboniferous formations, with over 37 new sinkholes reported since 2022. To address these risks, monitoring at the site includes an automatic seismic system, hydrogeological monitoring, regional geophysical surveys using gravimetry, complemented by ground geodetic observations and satellite InSAR studies to track surface uplift and subsidence. In addition, the Kazimierz-Juliusz mine, closed in 2016, has seen groundwater rise from -300 m to approximately +3.6 m above sea level over eight years following shaft backfilling and cessation of drainage. This may lead to uncontrolled sinkhole development, as observed at the Siersza mine. These changes are monitored through groundwater table measurements, gravity measurements, including surface geodetic measurements, and remote monitoring using InSAR satellite techniques.

Finally, partners from DMT-THGA conducts the InSAR processing for the Ruhr coal mine in North Rhine-Westphalia, Germany. According to the mine authority of North Rhine Westphalia, almost 2000 sinkholes occurred between 1986 and 2021, most of them directly related to former mining activities in areas with shallow overburden. The southern Ruhr area, where mining began in the 17th century, is particularly prone to sinkholes, with urban centres such as Dortmund, Bochum, Essen, and Duisburg still at risk, recent incidents in Bochum occurred beneath a school and in front of a hospital. InSAR application at this site will support the detection of sinkhole precursors and assessment of sinkholes hazard in this high-risk region. This report focuses on the InSAR processing of the Thil test site, the other sites will be presented in the next deliverable of the work package.

Figure 2: Mining sites studied with InSAR in the SIRIMA project

4. Working strategy and datasets

Both the Small Baseline Subset (SBAS) and Persistent Scatterer (PS) InSAR methods are applied at the different study sites using Sentinel-1 and TerraSAR-X data. Sentinel-1, a mission of Copernicus (Sentinel-1 | Copernicus Data Space Ecosystem), the European Union's Earth observation program, provides open and freely accessible C-band Synthetic Aperture Radar (SAR) imagery with a spatial resolution of approximately 5–20 m in Interferometric Wide (IW) mode. Sentinel-1A and Sentinel-1B satellites provide a 12-day revisit time each, and 6 days when both satellites are combined, which is crucial because the accuracy of deformation estimates increases with the number of SAR acquisitions, enabling the detection and monitoring of slow ground motions (<1 cm/year) with millimetric precision. On the other hand, higher-resolution X-band SAR data from TerraSAR-X mission (TerraSAR-X), operated by Airbus Defence and Space (DS) and German Space Agency (DLR), can be requested and accessed free of charge for scientific research projects. TerraSAR-X offers much finer spatial resolution (down to 3 m in strip map mode) and millimetre precision in interferometric measurements, though its temporal coverage is generally lower than Sentinel-1 due to less frequent acquisitions and its data are not available for all locations. TerraSAR-X data have already been requested and are available for the different study sites. Data acquisition has been confirmed for both the Thil (France) and Ruhr (Germany) mines.
The application of both methods (SBAS and PS) with Sentinel-1 and TerraSAR-X data will allow us to obtain both a regional overview of surface displacement and a more detailed, local view of deformation patterns, enabling the detection of subtle movements and potential sinkhole precursors at different spatial and temporal scales.

The methodology for InSAR-based monitoring of surface deformation within the SIRIMA project is presented in the following section (section 5), using the Thil mine as the representative test site. This work illustrates the processing and results obtained from Sentinel-1 data. The used tools might be different for the different partners (DMT-THGA, GIG-PIB) but the processing and the principles are the same. Details about the applied processing and the results on the other sites will be presented in the upcoming report.

5. InSAR methods applied for Thil test site

For the Thil test site, Sentinel-1 processing focused on a small portion of a single burst from the descending track 037 (Fig. 3A), as the area of interest is relatively small. All available Sentinel-1 acquisitions from this track, spanning November 2015 to April 2025, were included in the analysis. By combining acquisitions from Sentinel-1A and Sentinel-1B, we obtain an effective temporal resolution of one image every 6 days between mid-2017 and December 2021, when both satellites were operational. For the periods before mid-2017 (when only

Sentinel-1A was available) and after December 2021 (following Sentinel-1B's failure), the revisit time is 12 days.

A total of 443 Single Look Complex (SLC) images were co-registered using the Shuttle Radar Topography Mission (SRTM1) Digital Elevation Model (DEM; 30 m spatial resolution). Residual azimuth phase ramps were then removed from the co-registered SLCs, the processing area was reduced to a 15 km-wide region centred on Thil (Fig.3A), and the specific processing steps required for SBAS and PS analysis were carried out.

All InSAR processing for the Thil site was carried out using the GAMMA Remote Sensing software package (e.g., Wegmüller & Werner, 1998; Werner et al., 2000), which provides a complete set of tools for both SBAS processing and Persistent Scatterer analysis (through its IPTA-Interferometric Point Target Analysis- module).

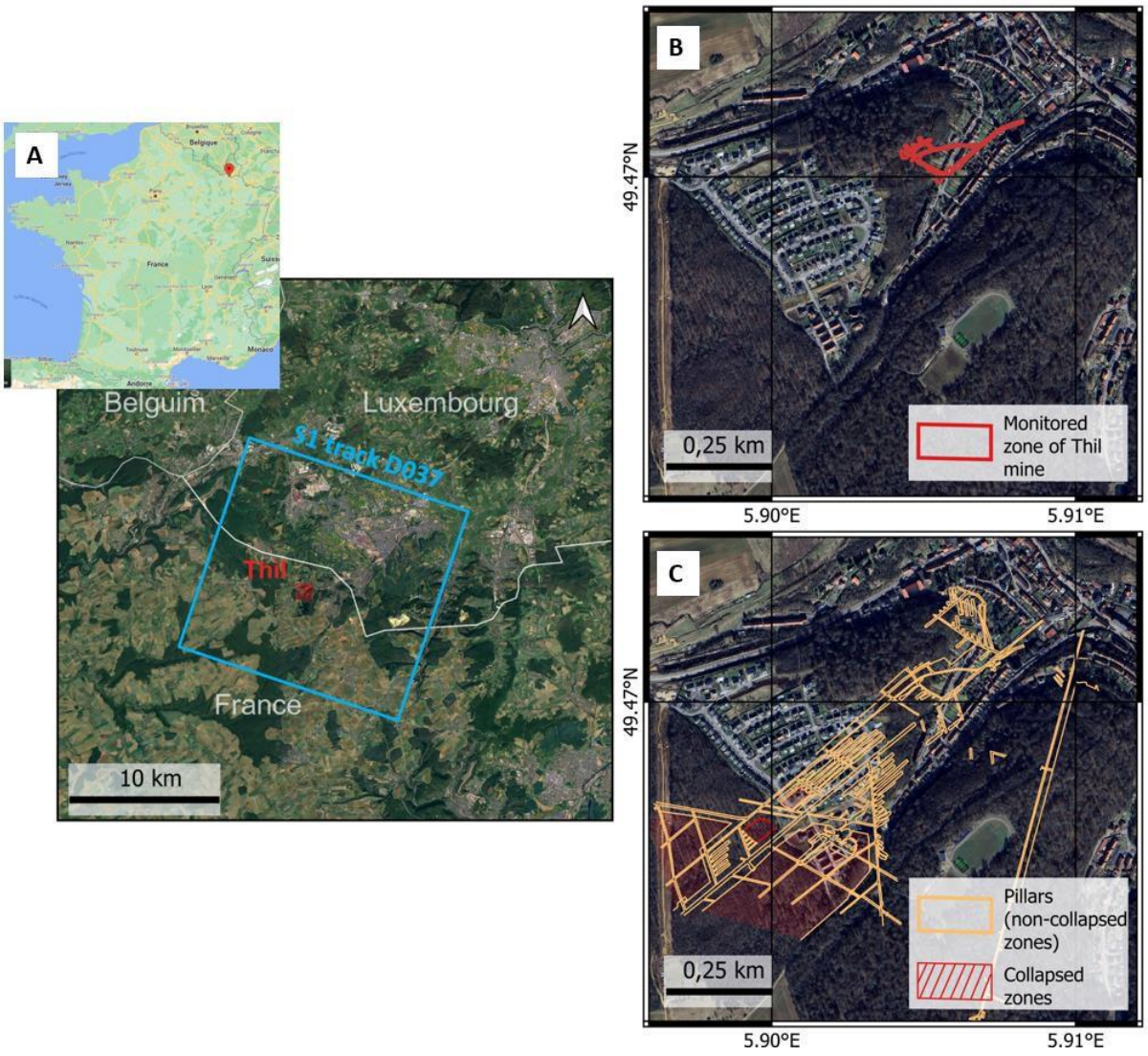

Figure 3: (A) Location of the Thil mine. (B) Zoom on the mining area showing the monitored section of the site. (C) Detailed view of the underground layout, highlighting accessible pillars and collapsed mining areas.

5.1. SBAS

SLCs were resampled by 6 in range and 1 in azimuth to get pixels of approximately 14 m spatial resolution for the SBAS processing. Then wrapped differential interferograms were computed at 6, 12, 18, 24 (Fig.4a) and 1 year (Fig.4b), when possible, where the STRM DEM was used to simulate the topographic phase component of each interferogram, which was then subtracted to isolate deformation and atmospheric signals.
The differential interferograms were spatially unwrapped using the Minimum Cost Flow (MCF) algorithm (Werner et al., 2002). To allow for the identification and correction of potential phase unwrapping errors, the redundant interferometric phases from the multi-reference acquisitions were combined into deformation time series using the multi-baseline (MB) approach without temporal smoothing, enabling the use of the modelled phase to correct unwrapping inconsistencies.
Once unwrapping consistency was verified, temporal smoothing was applied to the time series to recover non-linear deformation residuals that will be analysed to mitigate the atmospheric phase delay artifacts. A height-dependent atmospheric phase delay component, primarily due to stratified tropospheric effects, was modelled and removed by correlating the residual phase with topographic elevation. Turbulent atmospheric noise was then estimated from the smoothed phase residuals and corrected in both the wrapped and unwrapped interferograms. The multi-reference corrected unwrapped differential interferograms were subsequently used to estimate the deformation phase time series via a weighted least-squares algorithm that minimizes the sum of squared weighted residuals. From this time series, the average annual deformation rate over the nine-and-a-half-year observation period was computed.

5.2. Persistent Scatterer Interferometry with Interferometric Point Target Analysis (IPTA)

The followed IPTA processing is in accordance with the methodologies proposed in Wegmüller et al. (2004) and demonstrated in IPTA case studies (Gamma RS, 2005; Touski et al., 2019).
Processing continues with the oversampling of all co-registered SLCs by a factor of two in range to improve the estimation of interferometric phases at point targets. Candidate Persistent Scatterers (PS) were then identified using GAMMA's spectral-diversity and temporal-stability criteria, which exploit the temporal variability of backscattered amplitudes and the consistency of interferometric phases to isolate coherent radar target (Wegmüller et al., 2010). For each selected point target, differential interferometric phases were extracted, at 6, 12, 18, 24 and 1 year (Fig.4), after subtracting the topographic contribution derived from the SRTM DEM.
The phase histories of these points were then temporally unwrapped using a model-based approach that exploits the redundancy of the interferometric network to ensure phase consistency over time. This procedure estimates an initial linear deformation for each target and uses the obtained residual phases to isolate atmospheric path delays, separating height-

dependent (stratified) and turbulent components. After atmospheric correction, the set of corrected unwrapped differential phases was inverted using a multi-baseline least-squares approach to retrieve a consistent time series of deformation for each point target.

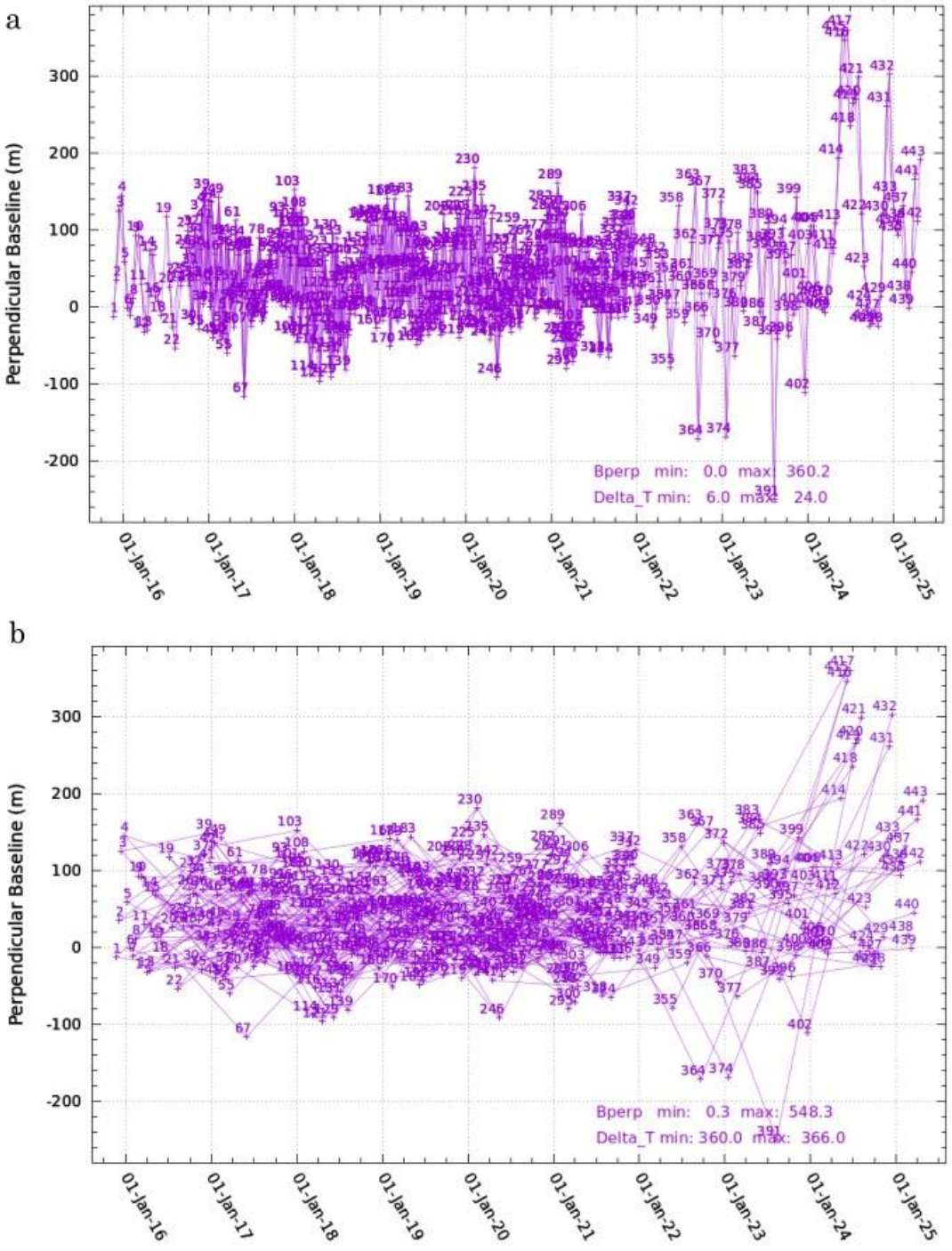

Figure 4: Temporal and perpendicular baselines of the generated Sentinel-1 interferograms for both SBAS and IPTA processing over the study area, showing the interferogram network of (a) 6-, 12-, 18-, and 24-day intervals, and (b) 1-year interval.

6. Preliminary results on Thil test site

The following figures present the LOS mean velocity maps obtained from both SBAS and IPTA processing for the 2015–2025 period. The convention of negative and positive values has been inverted so that negative values correspond to motion away from the satellite, while positive values indicate motion toward the satellite.

From SBAS processing, the basin appears mostly stable, with average velocities between -1 and 1 mm/year (Fig.5). Very small subsidence values (motion away from the satellite) of around 2–3 mm/year are observed in certain parts of the mined areas. However, local analysis of the displacement with those results is challenging due to the pixel size relative to the scale of the mining and risk zones (Fig. 6).

The average velocities of the persistent scatterers obtained from IPTA processing (Figs. 7 and 8) confirm that the basin is mostly stable, with velocities ranging from -1 to 1 mm/year. However, some localized deformation areas are highlighted at the building scale, with accelerated movements occurring within the mining areas, where some of these coincide with risk zones identified by the DPSM (Fig.8). It is important to note that the spatial positioning accuracy of the persistent scatterers is limited by the SAR ground resolution, which is approximately 5 m in range and 20 m in azimuth.

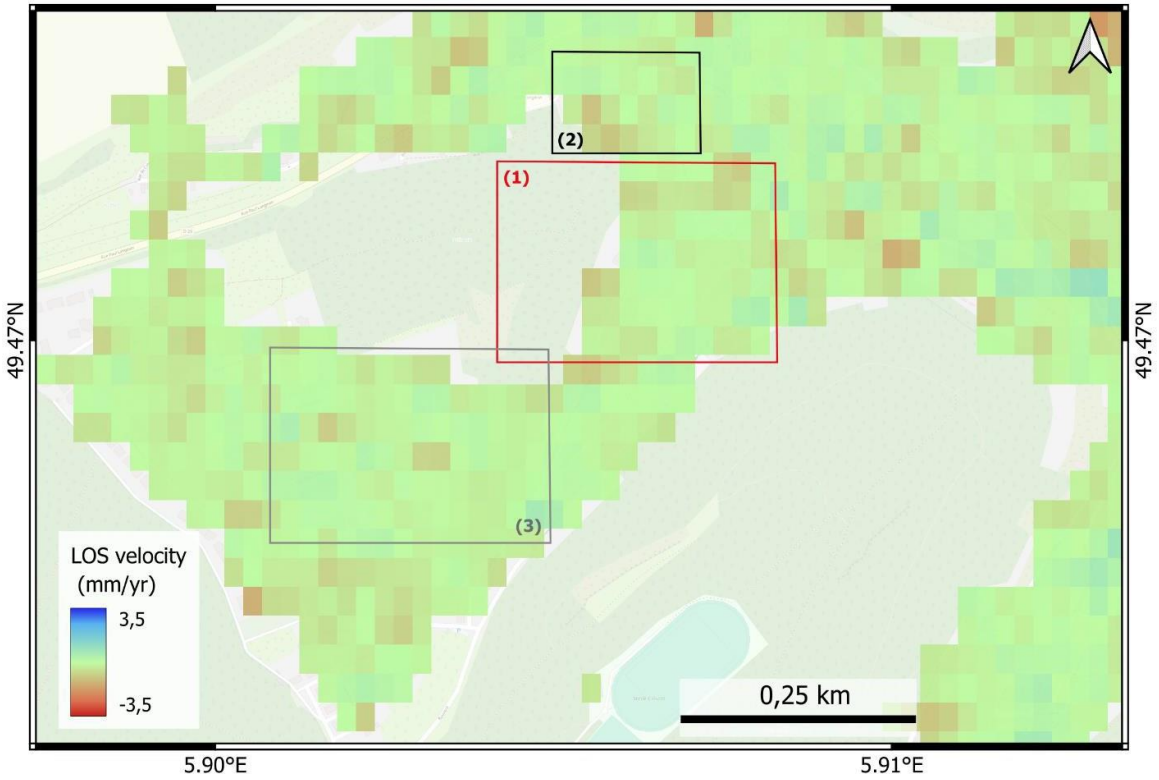

Figure 5: LOS mean velocity map for the 2015–2025 period obtained with SBAS processing. Negative values indicate motion away from the satellite. The zoomed areas correspond to the regions shown in Figures 9, 12, and 15.

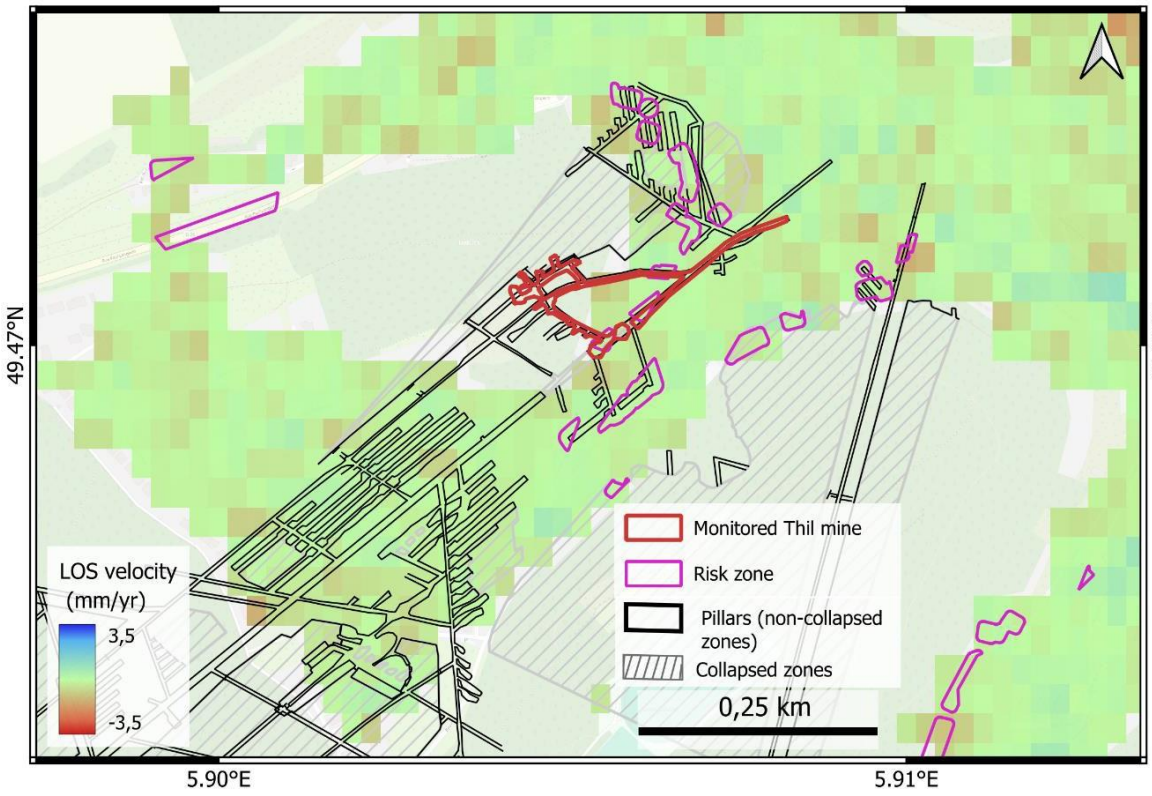

Figure 6: LOS mean velocity map for the 2015–2025 period obtained with SBAS processing, overlaid with the available underground mine layout with the risk zones identified by the DPSM. Negative values indicate motion away from the satellite.

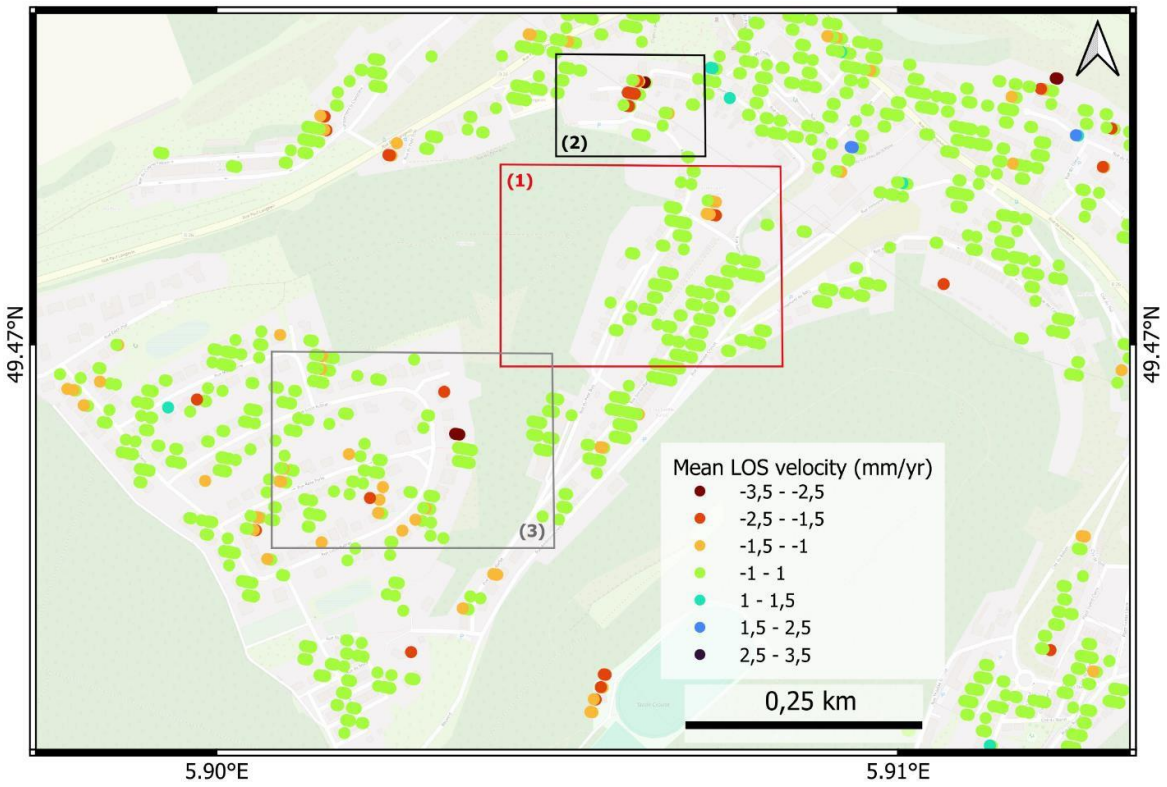

Figure 7 : LOS mean velocity map for the 2015–2025 period obtained with IPTA processing. Negative values indicate motion away from the satellite. The zoomed areas correspond to the regions shown in Figures 10, 13, and 16.

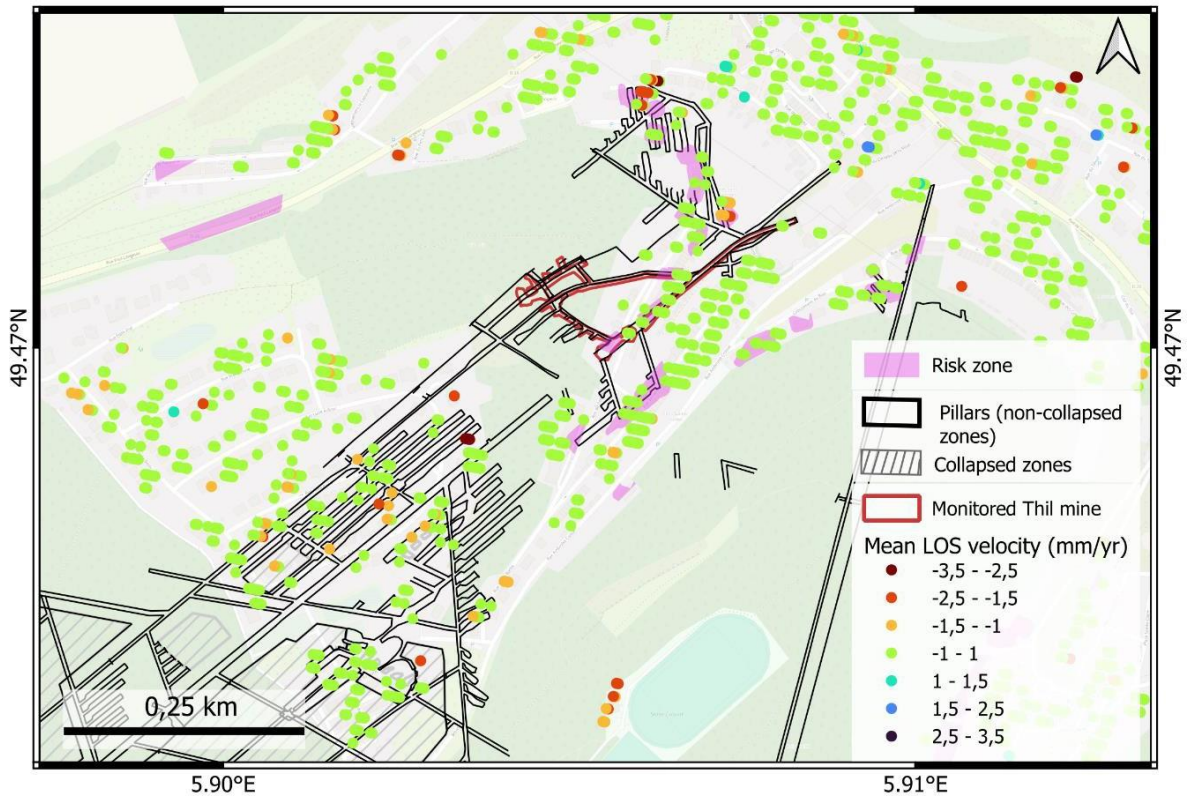

Figure 8: LOS mean velocity map for the 2015–2025 period obtained with IPTA processing, overlaid with the available underground mine layout with the risk zones identified by the DPSM. Negative values indicate motion away from the satellite.

Focusing on the monitored zone of the Thil mine, the persistent scatterers located within the buffer zone show LOS velocity close to zero (Fig. 10). Their corresponding displacement time series also do not exhibit any specific deformation trend (Fig. 11a, b).

In these preliminary results, there is no persistent scatterers over the western cavity of the monitored Thil mine, where roof collapses have been reported (Fig. 10). This is likely due to the vegetation coverage in this area, which reduces the coherence between different SAR acquisitions. Further processing is ongoing to assess whether a reliable time series can be obtained with an acceptable signal-to-noise ratio at this location. Higher-resolution data (e.g., TerraSAR-X) will be valuable for capturing deformation signals along the nearby road above the cavity. However, the SBAS results do not show evidence of movement in the vicinity of either of the two cavities (Fig.9).

In contrast, to the north of the monitored mining area, several PS show localized increase of velocity within one of the identified risk zones (Fig.10), corresponding to a house currently monitored by the DPSM. The displacement time-series at this location reveals a distinct pattern (Fig.11c): the motion was mostly stable prior to 2019, aside from an event occurring around August 2018, followed by a clear increase of velocity of approximately 5 mm/year from 2019 onward, which continues to the present day.

Further investigation of localized velocity increase detected by persistent scatterers within another risk zone located north of the mining area (Fig. 13, corresponding to Zoom 2 in Fig. 7) shows that the displacement appears to be associated with a specific event around March–

April 2021 (Fig.14). Additional analysis and coordination with the DPSM will be necessary to better understand the cause of this sudden change observed at this location.

Additional examples are found in the southern part of the mining area (Fig. 16, Zoom 3 of Figure 7), where mining pillars persist. The time-series of several points show localized increase of velocity occurring during specific periods (Fig.16, 17a, b). These displacement patterns also require further investigation to assess whether they can be linked to reported events or known ground instabilities in the area.

Not all PS time-series offer clear deformation trends, particularly when the analysis relies on a single PS. In some cases, the signal can be quite noisy (e.g., Fig. 17c), making the analysis of deformation trends more challenging.

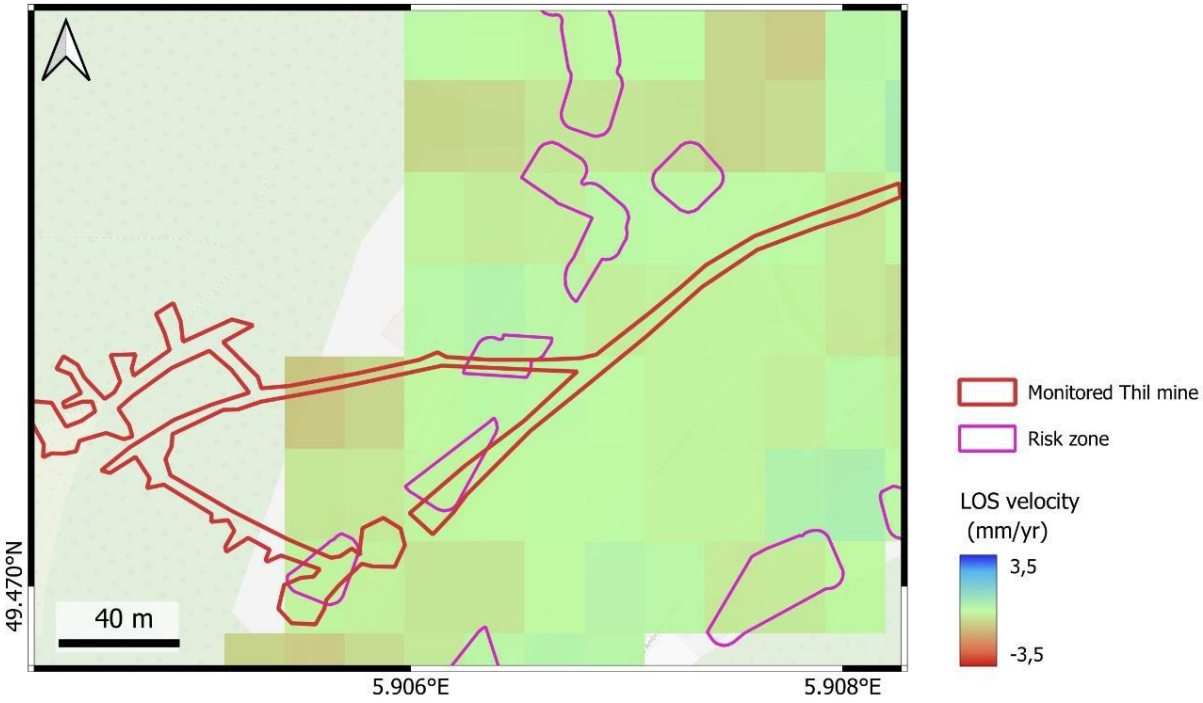

Figure 9: Zoom showing the LOS mean velocity map for the 2015–2025 period obtained from SBAS processing, overlaid with the monitored section of the Thil mine and the risk zones. The location of this zoomed area is indicated by polygon 1 in Figure 5.

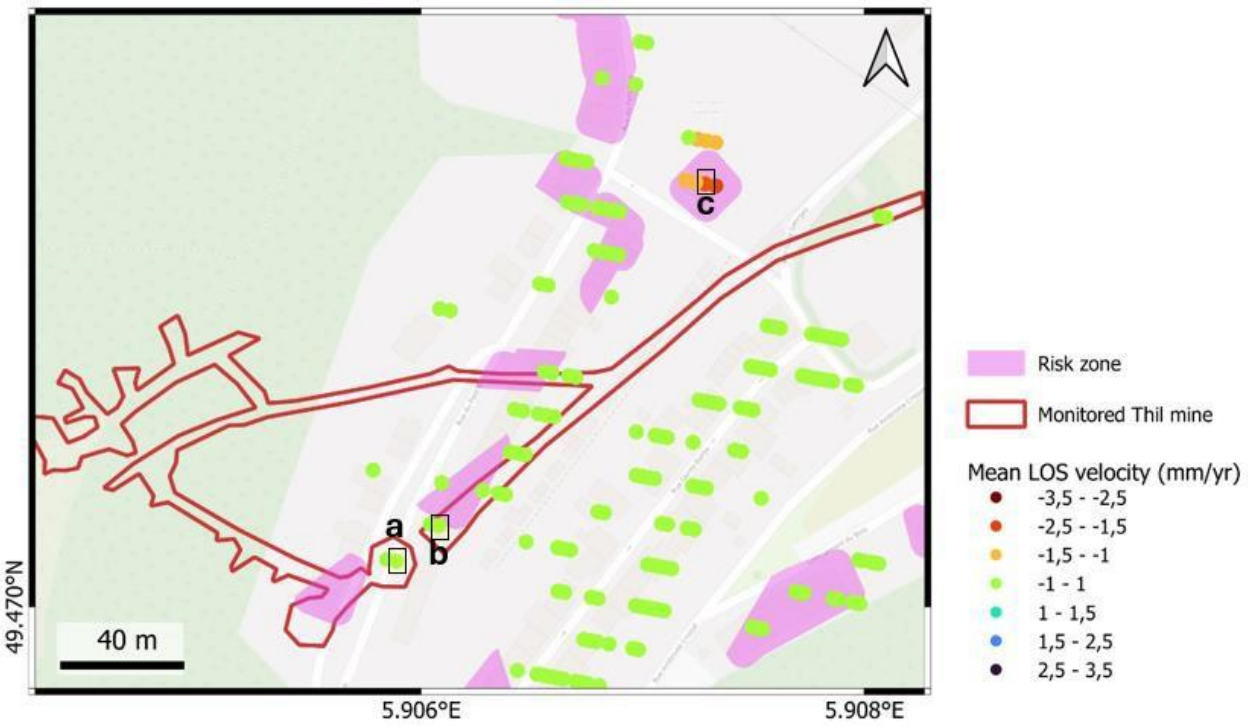

Figure 10: Zoom showing the LOS mean velocity map for the 2015–2025 period obtained with IPTA processing, overlaid with the monitored section of the Thil mine and the risk zones. The location of this zoomed area is indicated by polygon 1 in Figure 7. Points a, b and c indicate the locations of the time series presented in Figure 11.

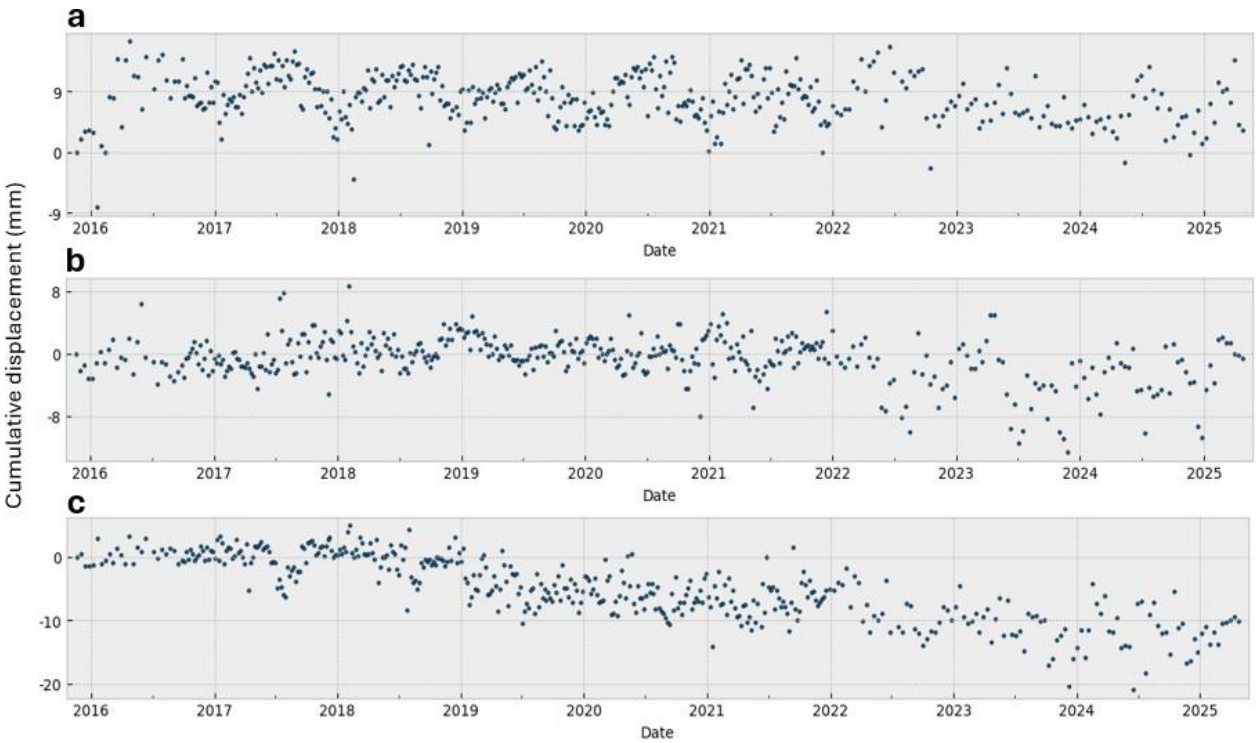

Figure 11: Time series plots showing the cumulative LOS displacement for points a, b and c indicated in Figure 10.

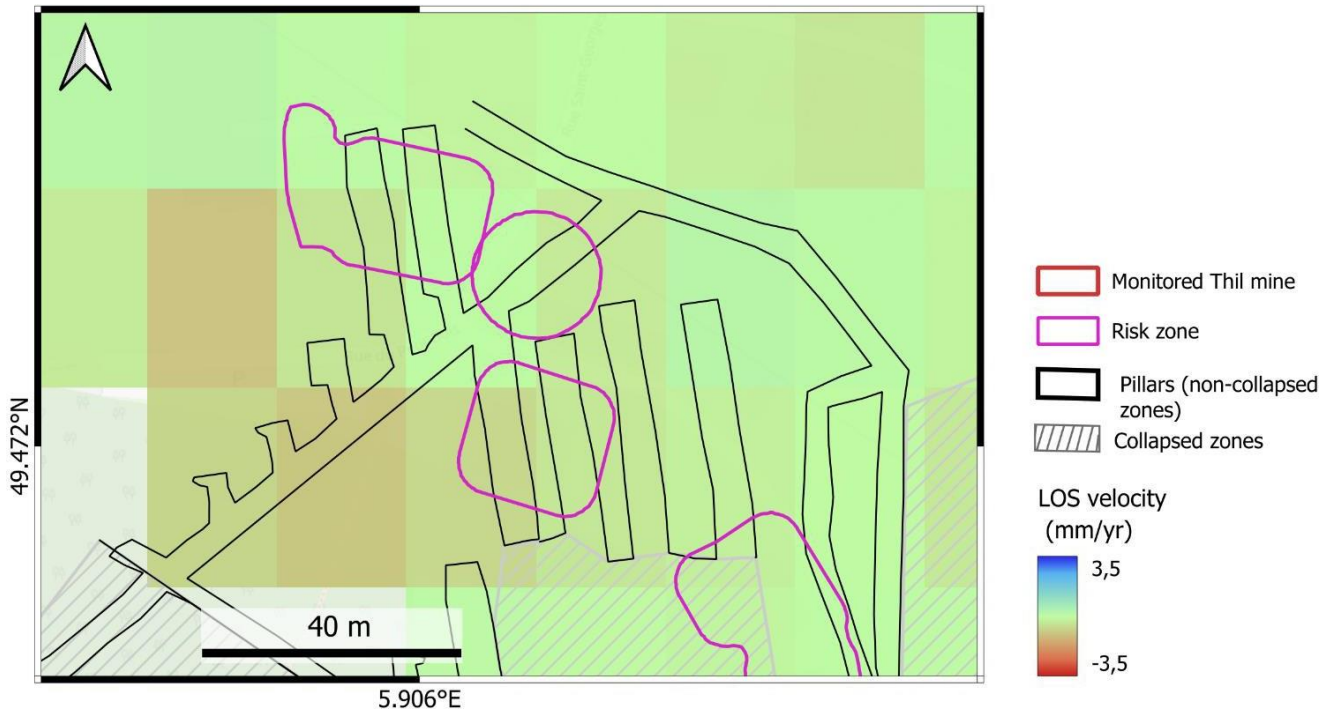

Figure 12: Zoom showing the LOS mean velocity map for the 2015–2025 period obtained from SBAS processing, overlaid with the available underground mine layout and the risk zones. The location of this zoomed area is indicated by polygon 2 in Figure 5.

Figure 13: Zoom showing the LOS mean velocity map for the 2015–2025 period obtained with IPTA processing, overlaid with the available underground mine layout and the risk zones. The location of this zoomed area is indicated by polygon 2 in Figure 7. Points a, b and c indicate the locations of the time series presented in Figure 14.

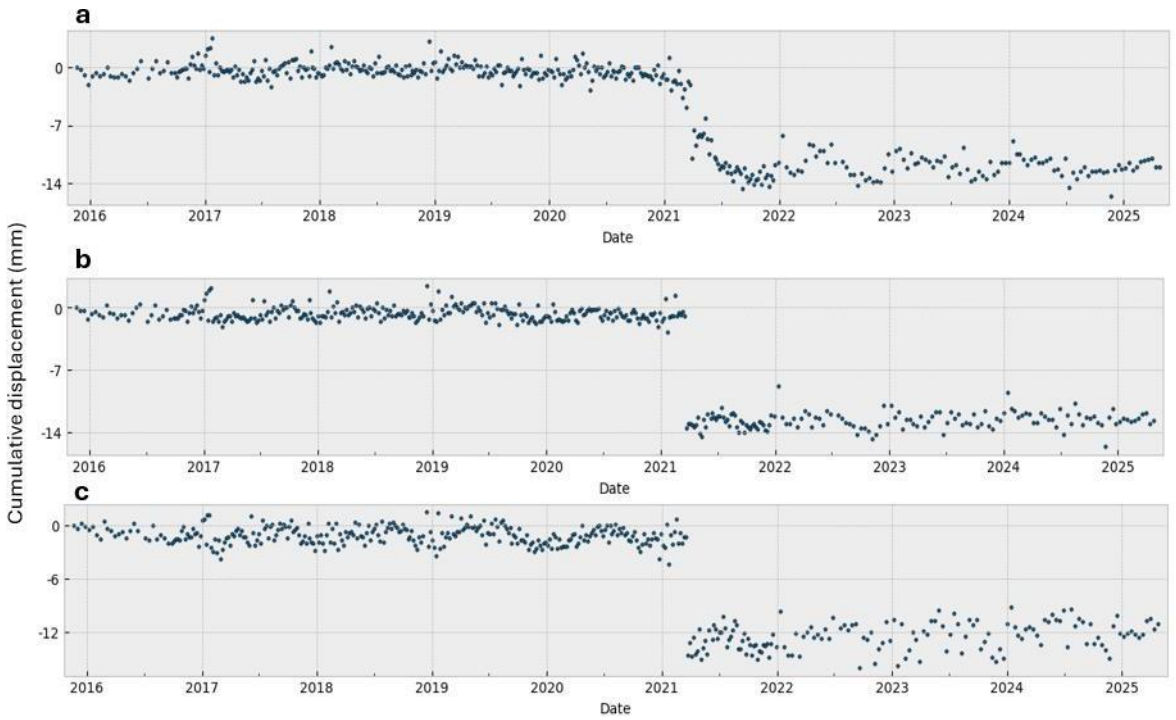

Figure 14: Time series plots showing the cumulative LOS displacement for points a, b and c indicated in Figure 13.

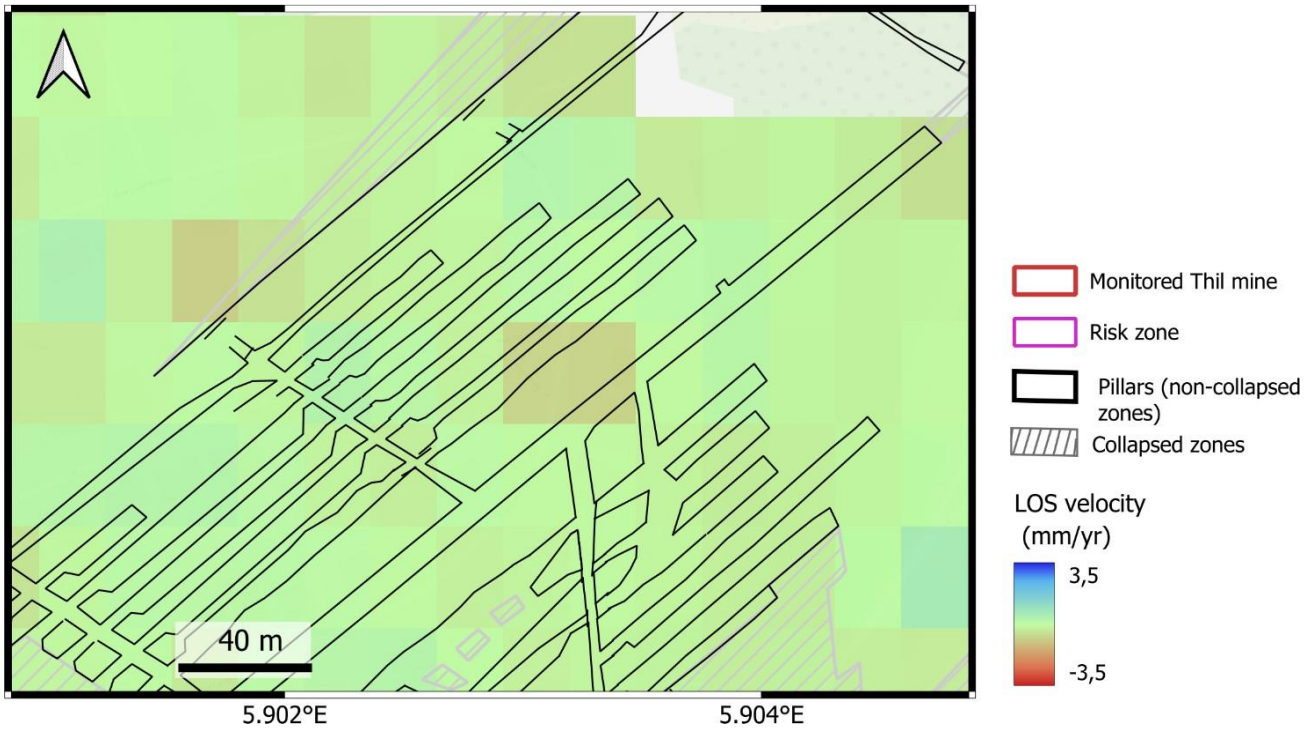

Figure 15: Zoom showing the LOS mean velocity map for the 2015–2025 period obtained from SBAS processing, overlaid with the available underground mine layout and the risk zones. The location of this zoomed area is indicated by polygon 3 in Figure 5.

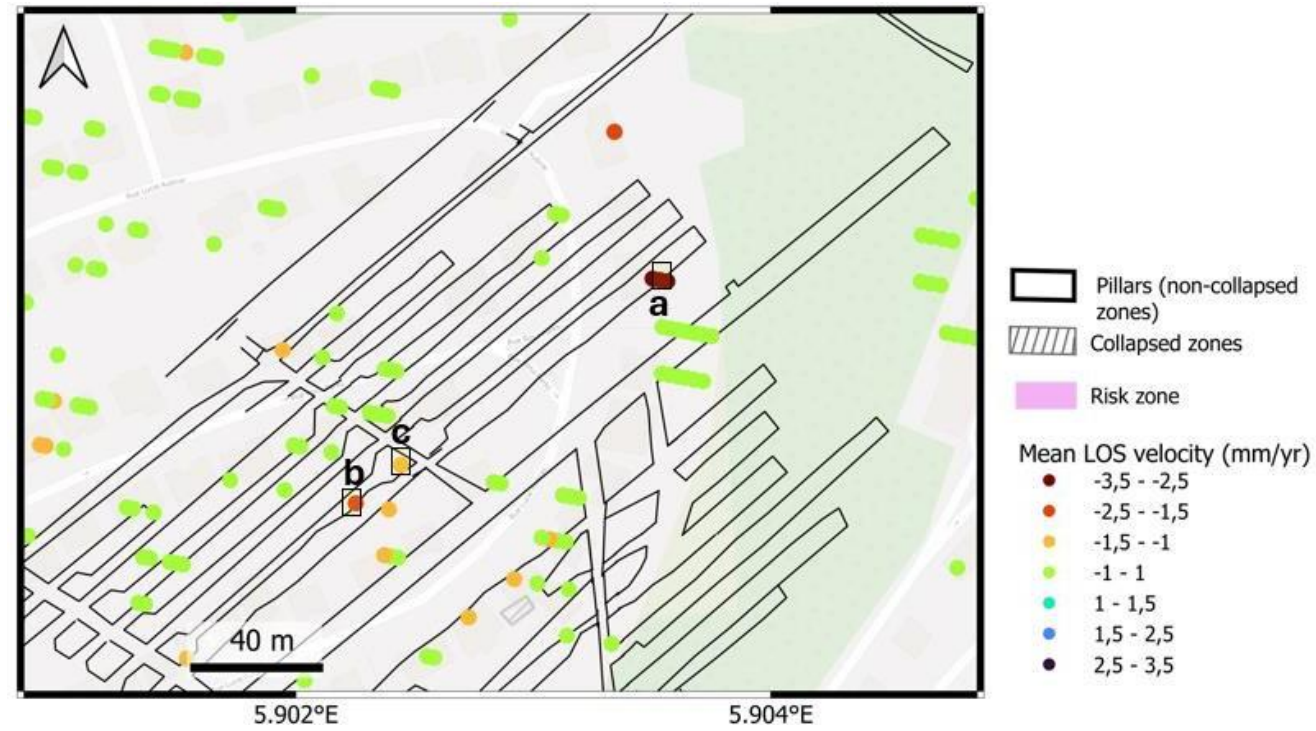

Figure 16: Zoom showing the LOS mean velocity map for the 2015–2025 period obtained with IPTA processing, overlaid with the available underground mine layout and the risk zones. The location of this zoomed area is indicated by polygon 3 in Figure 7. Points a, b and c indicate the locations of the time series presented in Figure 17.

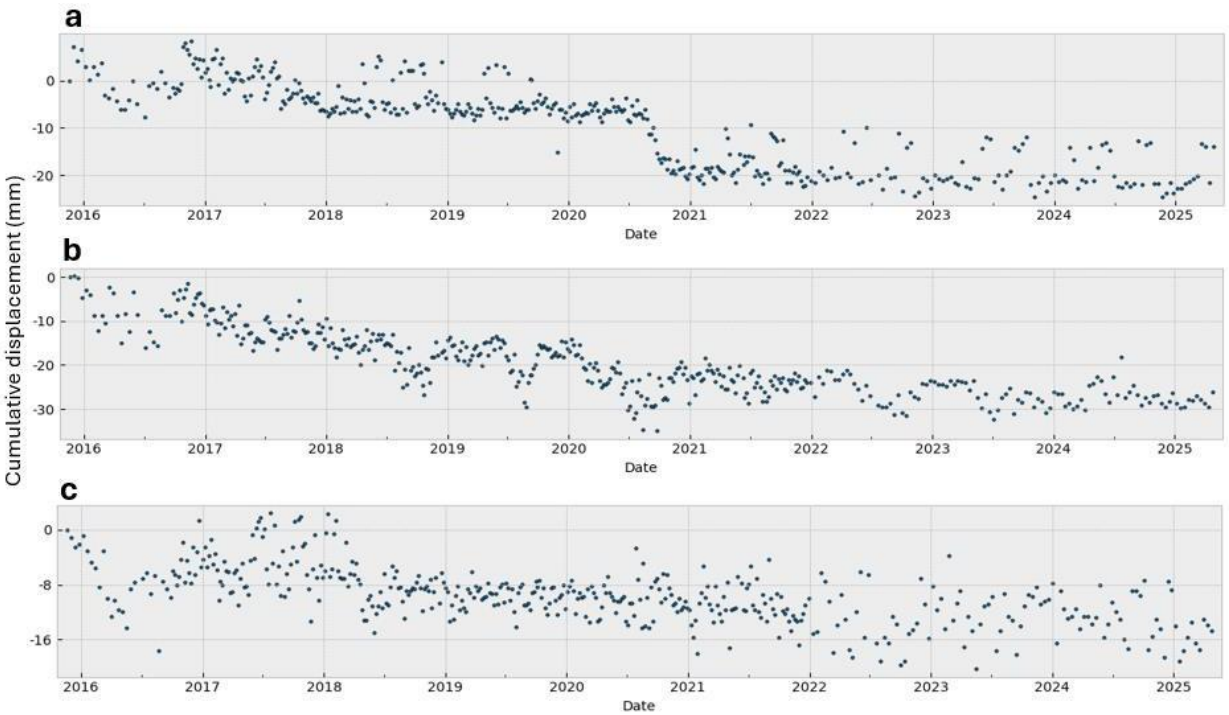

Figure 17: Time series plots showing the cumulative LOS displacement for points a, b and c indicated in Figure 16.

7. The introduction of a new study site in France: Saint-Etienne mining site

The preliminary analysis of InSAR with the full archive of Sentinel-1 data, from November 2015 to April 2025, on the Thil site using both Small Baseline Subset (SBAS) and Persistent Scatterer (PS) InSAR methods, revealed no significant displacement in the area affected by the roof falls. Our concern is that this collapse, which occurred at an unknown date between 2018 and 2020, was only identified during BRGM's annual inspection of the gallery, having gone unnoticed by the local population due to the absence of visible surface effects. The lack of InSAR signal from Sentinel-1 data is likely due to the absence of rapid enough (> 2 mm/yr) or large enough surface deformation to be detected. Consequently, even with higher-resolution data like TerraSAR-X, the potential to observe meaningful movement remains uncertain.

It was brought to our attention that another more promising site from an InSAR processing perspective is in Saint-Étienne where a mining-induced sinkhole occurred. Saint-Étienne is a former hard coal mining area, making it more suitable for the objectives of the SIRIMA project. On the night of March 2 to 3, 2021, a sinkhole emerged at the surface near a commercial building, in the Loire department. Approximately ten meters in diameter, the sinkhole caused visible surface damage and directly impacted the building. The sinkhole site is well-documented and linked to the former coal mining activity in the area.

Investigation of the site using the European Ground Motion Service interface (Fig. 18) shows an acceleration during the three months preceding the sinkhole, which could potentially be interpreted as a precursor to the event. Therefore, we propose to conduct InSAR analysis at the Saint-Étienne site, more suitable for studying the sinkhole event. This analysis will allow us to investigate possible precursory deformation leading up to the event and to better understand the spatial extent of ground instability. For example, by analysing time series up to the date of the sinkhole separately from the post-event motion to isolate the precursor signals. Unfortunately, no TerraSAR-X data are available for this site.

Since a building was directly affected, the results on the Saint-Etienne mine will also support the assessment of building vulnerability in response to such movements, contributing directly to the other objectives of the SIRIMA project.

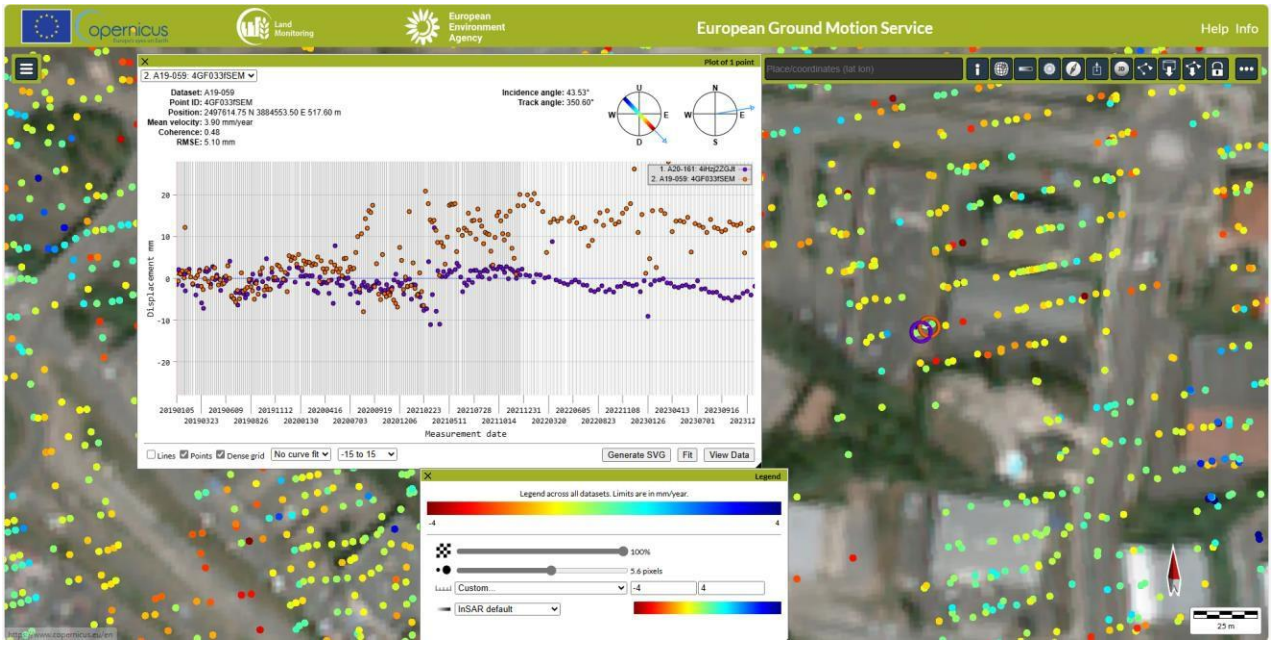

Figure 18: Persistent scatterers from the European Ground Motion Service at the Saint-Étienne site (ascending tracks 161 and 59 of Sentinel-1 data). Negative values indicate motion away from the satellite.

8. Conclusions and perspectives

This deliverable presented the InSAR methodology applied within the SIRIMA project for monitoring hard coal post-mining areas. The Thil mine was used as a representative test site to demonstrate the methodology, which will also be applied to four additional sites: the Siersza and Kazimierz-Juliusz mines in Poland, the Ruhr mine in Germany, and the Saint-Étienne mining site in France.

The preliminary results from the processing of Sentinel-1 SAR data at Thil revealed several areas of local deformation, primarily associated with former mining activities, some of which correspond to risk zones identified by the Department of Mine Safety and Risk Prevention (BRGM-DPSM). Combining the InSAR-detected localised velocity increase with available DPSM records will help validate the relationship between observed surface movements and past mining activities. Further investigations are needed for this purpose.

The next step for Thil study site is to process higher-resolution TerraSAR-X data to detect localized ground deformations linked to the 2018–2020 roof falls and confirm previously observed local deformations with Sentinel-1, providing key insights for post-mining monitoring. In parallel, the Saint-Étienne site in France will be processed, offering the opportunity to investigate a mining-related sinkhole and identify potential precursory ground movements.

InSAR studies are ongoing at the other study sites led by the GIG-PIB and DMT-THGA partners. Unlike the French sites, the Polish and German sites have experienced a significant number of sinkholes in recent years, the same period covered by InSAR processing.

Consequently, InSAR monitoring at these locations increases the potential to detect and understand precursory signals associated with sinkhole formation. This will contribute to a comprehensive database for comparative analysis across all study sites. The detailed methodology and results for each site will be presented in the next deliverable.

References

Albino, F., Biggs, J., Yu, C., & Li, Z. (2020). Automated methods for detecting volcanic deformation using Sentinel-1 InSAR time series illustrated by the 2017–2018 unrest at Agung, Indonesia. *Journal of Geophysical Research: Solid Earth*, 125, e2019JB017908. **https://doi.org/10.1029/2019JB017908**

Apanowicz, B., Milczarek, W., and Kowalski, A. (2025). Advanced InSAR-SBAS method for determining the extent of mining-induced deformations. Geocarto International. 40. 10.1080/10106049.2025.2523428.

Aslan, G.; Foumelis, M.; Raucoules, D.; De Michele, M.; Bernardie, S.; Cakir, Z. (2020) Landslide Mapping and Monitoring Using Persistent Scatterer Interferometry (PSI) Technique in the French Alps. *Remote Sens.*, *12*, 1305. https://doi.org/10.3390/rs12081305

Berardino P., Fornaro G., Lanari R. and Sansosti E. (2002), "A new algorithm for surface deformation monitoring based on small baseline differential SAR interferograms," in *IEEE Transactions on Geoscience and Remote Sensing*, vol. 40, no. 11, pp. 2375-2383, Nov. 2002, doi: 10.1109/TGRS.2002.803792.

Biggs, J., & Pritchard, M. E (2017). Global volcano monitoring: What does it mean when volcanoes deform? *Elements, 13*(1), 17–22. https://doi.org/10.2113/gselements.13.1.17

Boullée, H. (2022). *Bassin ferrifère lorrain – Suivi 2021 des zones bâties à risques de fontis – Commune de Thil (54880).* Rapport final. BRGM/RP-71337-FR, 80 p., 4 fig., 21 ann. dont 1 sur USB.

Cheaib, A., Lacroix, P., Zerathe, S., Jongmans, D., Ajorlou, N., et al. (2022), Landslides induced by the 2017 Mw7.3 Sarpol Zahab earthquake (Iran). *Landslides*, 19 (3), pp.603-619. ⟨10.1007/s10346-021-01832-0⟩.

Crosetto M, Solari L, Balasis-Levinsen J, Bateson L, Casagli N, Frei M, Oyen A, Moldestad DA, Mróz M (2021) Deformation monitoring at European scale: the Copernicus Ground Motion Service. International Archives of the Photogrammetry, Remote Sensing and Spatial Information Sciences, XLIII-B3-2021, 141–146. https:// doi. org/ 10. 5194/ isprs- archi ves- XLIII- B3- 2021- 141- 2021

de Michele, M., Raucoules, D., Rault, C., Aunay, B., and Foumelis, M. (2023), Short communication: Potential of Sentinel-1 interferometric synthetic aperture radar (InSAR) and offset tracking in monitoring post-cyclonic landslide activities on Réunion, Earth Surf. Dynam., 11, 451–460. https://doi.org/10.5194/esurf-11-451-2023

Doin, M.-P., Lodge, F., Guillaso, S., Jolvet, R., Lasserre, C., Ducret, G., et al. (2011). Presentation of the small baseline NSBAS Processing chain on a case example: The Etna deformation monitoring from 2003 to 2010 using Envisat data. Proc. esaFringe.

Ferretti, A., Prati, C., and Rocca, F. (2001), "Permanent scatterers in SAR interferometry," in *IEEE Transactions on Geoscience and Remote Sensing*, vol. 39, no. 1, pp. 8-20. doi: 10.1109/36.898661

Gamma RS. (2005). ERS–ASAR integration in GAMMA IPTA processing. Technical Report, Gamma Remote Sensing, Switzerland.

Hanssen, R.F. (2001) Radar Interferometry: Data Interpretation and Error Analysis. Kluwer Academic, Dordrecht, Boston. https://doi.org/10.1007/0-306-47633-9

Herrera, G., Tomás, R., Vicente, F., Lopez-Sanchez, J.M., Mallorquí, J.J. , Mulas, J. (2010), Mapping ground movements in open pit mining areas using differential SAR interferometry, International Journal of Rock Mechanics and Mining Sciences, 47(7), 1114-1125, ISSN 1365-1609. https://doi.org/10.1016/j.ijrmms.2010.07.006

Hooper, A., H. Zebker, P. Segall, and B. Kampes (2004), A new method for measuring deformation on volcanoes and other natural terrains using InSAR persistent scatterers, *Geophys. Res. Lett.*, 31, L23611, doi:10.1029/2004GL021737.

Lanari, R., Mora, O., Manunta, M., Mallorqui, J. J. , Berardino, P. and Sansosti, E. (2004), "A small-baseline

approach for investigating deformations on full-resolution differential SAR interferograms," in *IEEE Transactions on Geoscience and Remote Sensing*, vol. 42, no. 7, pp. 1377-1386. doi: 10.1109/TGRS.2004.828196

Massonnet, D. & Feigl, K. L. (1998), Radar interferometry and its application to changes in the Earth's surface. Rev. Geophys. 36, 441-500. Reviews of Geophysics. 36. 10.1029/97RG03139.

Massonnet, D., Rossi, M., Carmona, C. *et al.* (1993), The displacement field of the Landers earthquake mapped by radar interferometry. *Nature* **364**, 138–142. https://doi.org/10.1038/364138a0

Raucoules D., Colesanti C. and Carnec C, (2007), *Use of SAR interferometry for detecting and assessing ground subsidence*, Compte Rendus Geosciences, vol 339, n°5, p 289

Rosi, A., Tofani, V., Tanteri, L. *et al.* (2018), The new landslide inventory of Tuscany (Italy) updated with PS-InSAR: geomorphological features and landslide distribution. *Landslides* **15**, 5–19. https://doi.org/10.1007/s10346-017-0861-4

Small, D. 1998. Generation of digital elevation models through spaceborne SAR Interferometry. 1998. PhD thesis, University of Zürich.

Touski, M. Y., Veiskarami, M., & Dehghani, M. (2019). Interferometric Point Target Analysis (IPTA) for landslide monitoring Int. Arch. Photogramm. Remote Sens. Spatial Inf. Sci., XLII-4/W18, 1079–1083, https://doi.org/10.5194/isprs-archives-XLII-4-W18-1079-2019

Wegmüller, U., & Werner, C. L. (1998). SAR processing, interferometry, differential interferometry and geocoding software. InEuropean conference on Synthetic Aperture Radar, EUSAR98, Friedrichshafen, Germany, 25-27 May 1998.

Wegmüller, U. & Strozzi, T. & Wiesmann, Andreas. (2004). Multi-temporal interferometric point target analysis. Series in Remote Sensing. 3. 136-144. 10.1142/9789812702630_0015

Wegmuller, U., Walter, D., Spreckels, V., and Werner, C. L. (2010), "Nonuniform Ground Motion Monitoring With TerraSAR-X Persistent Scatterer Interferometry," in *IEEE Transactions on Geoscience and Remote Sensing*, vol. 48, no. 2, pp. 895-904. doi: 10.1109/TGRS.2009.2030792

Werner, C., Wegmüller, U., Strozzi, T., & Wiesmann, A. (2000). GAMMA SAR and Interferometric Processing Software. Presented at the ERS ENVISAT Symposium, Gothenburg, Sweden, 16–20 October 2000.

Werner, C., Wegmüller, U., Strozzi, T. and Wiesmann, A. (2002), Processing strategies for phase unwrapping for INSAR applications, Proceedings.EUSAR 2002, Cologne, 4-6 June, 2002.

Wright, T. J., Parsons, B., & Fielding, E. J. (2001). Measurement of interseismic strain accumulation across the North Anatolian Fault by satellite radar interferometry. *Geophysical Research Letters, 28(10*), 2117-2120.